AJNR

# MR Imaging of Metronidazole-Induced Encephalopathy: Lesion Distribution and Diffusion-Weighted Imaging Findings

E. Kim, D.G. Na, E.Y. Kim, J.H. Kim, K.R. Son and K.H. Chang



*AJNR Am J Neuroradiol* published online 20 September 2007
http://www.ajnr.org/content/early/2007/09/20/ajnr.A0655.citation

Published September 18, 2007 as 10.3174/ajnr.A0655

ORIGINAL RESEARCH

# MR Imaging of Metronidazole-Induced Encephalopathy: Lesion Distribution and Diffusion-Weighted Imaging Findings

E. Kim
D.G. Na
E.Y. Kim
J.H. Kim
K.R. Son
K.H. Chang

**BACKGROUND AND PURPOSE:** MR imaging features of metronidazole-induced encephalopathy (MIE) have not been fully established. This study was undertaken to determine the topographic distributions and diffusion-weighted imaging (DWI) findings of MIE.

**MATERIALS AND METHODS:** We retrospectively evaluated the initial MR images ($n = 7$), including DWI ($n = 5$), and follow-up MR images ($n = 4$) after drug discontinuation in 7 patents with clinically diagnosed MIE. The topographic distributions of lesions were evaluated on MR images, and DWI signal intensities and apparent diffusion coefficient (ADC) values of the lesions were assessed.

**RESULTS:** MR images demonstrated bilateral symmetric T2 hyperintense lesions in the cerebellar dentate nucleus ($n = 7$), midbrain ($n = 7$), dorsal pons ($n = 6$), medulla ($n = 4$), corpus callosum ($n = 4$), and cerebral white matter ($n = 1$). Brain stem lesions involved the following: tectum ($n = 5$), tegmentum ($n = 4$), red nucleus ($n = 3$) of the midbrain, vestibular nucleus ($n = 6$), and a focal tegmental lesion involving the superior olivary nucleus ($n = 6$) and abducens nucleus ($n = 4$) of the pons and vestibular nucleus ($n = 4$) and inferior olivary nucleus ($n = 1$) of the medulla. DWI ($n = 5$) showed isointensity or hyperintensity of lesions, and the decreased ADC value was found only in the corpus callosum lesions ($n = 2$). All detected lesions were completely reversible at follow-up except for the single corpus callosum lesion with an initial low ADC value.

**CONCLUSION:** Brain lesions were typically located at the cerebellar dentate nucleus, midbrain, dorsal pons, medulla, and splenium of the corpus callosum. According to DWI, most of the lesions in MIE probably corresponded to areas of vasogenic edema, whereas only some of them, located in the corpus callosum, corresponded to cytotoxic edema.

Metronidazole-induced encephalopathy (MIE) is a rare toxic encephalopathy caused by the antibiotic drug metronidazole. Metronidazole is a nitroimidazole antibiotic and has been available for clinical use for more than 30 years, and it has played an important role in anaerobic-related infections and for preventing or retarding the development of clinical recurrence in Crohn disease. Metronidazole has good cellular penetration and is believed to penetrate CSF and the central nervous system easily.[1] It is also comparatively safe when used at appropriate dosages, but it can produce peripheral neuropathies and cerebellar dysfunction, especially at dosages exceeding 2 g/day for prolonged periods.[2,3] The incidence of MIE is unknown, though several previous studies have addressed brain change caused by metronidazole neurotoxicity.[2-16] To our knowledge, several reports on 13 patients with MIE have documented MR brain imaging of abnormalities,[7-16] and diffusion-weighted imaging (DWI) data have been presented for 3 patients with MIE.[11,12,14] Previous case reports have focused on cerebellar lesions, and little radiologic investigation of MR imaging findings with respect to brain stem pathology and topographic lesion distribution has been performed in patients with MIE.

This study was performed to determine the topographic distributions of lesions demonstrated on MR images and to document the DWI findings of brain lesions in patients with MIE.

Received February 7, 2007; accepted after revision March 12.

From the Department of Radiology and Institute of Radiation Medicine (E.K., D.G.N., K.H.C., K.R.S.), Seoul National University College of Medicine, Seoul, Korea; the Department of Radiology (E.K.), Samsung Medical Center, Sungkyunkwan University School of Medicine, Seoul, Korea; the Department of Radiology (E.Y.K.), Research Institute of Radiologic Science, Yonsei University College of Medicine, Seoul, Korea; and the Department of Radiology (J.H.K.), Seoul Metropolitan Boramae Hospital, Seoul, Korea.

Please address correspondence to Dong Gyu Na, MD, Department of Radiology and Institute of Radiation Medicine, 28 Yongon-dong, Chongno-gu, Seoul, 110-744, Korea; e-mail: dgna@radiol.snu.ac.kr

DOI 10.3174/ajnr.A0655

## Materials and Methods

### *Patients*

This study included 7 patients in whom the final clinical diagnosis was MIE, during a period of 4 years. There were 6 men and 1 woman, and the mean age of patients was 61 years (range, 49–71 years). Final clinical diagnoses of MIE were determined on the basis of probable adverse drug reactions to conventional categories of adverse drug reactions.[17] All patients had been administered metronidazole therapy for several weeks before their neurologic signs and symptoms were developed. When MIE was clinically suspected, metronidazole medication was stopped in all patients. Thiamine had not been previously administered to any of the 7 patients during the clinical course. Medical records were reviewed to assess clinical parameters, such as total metronidazole dose, duration of administration, duration of symptom onset after administration, neurologic symptoms and signs, and duration of recovery after discontinuation.

### *MR Imaging*

All 7 patients underwent MR imaging after symptom onset. DWI was performed in 5 patients, and follow-up MR imaging after metronidazole discontinuation, in 4 patients. MR imaging was performed by using 1.5T MR imaging systems (Sonata, Siemens, Erlangen, Germany; Signa Horizon and Genesis Signa, GE Healthcare, Milwaukee, Wis; Gyroscan Intera, Philips, Best, the Netherlands). Spin-echo T1-

**Table 1: Demographic and clinical data of seven patients with MIE**

| Patient | Age/Sex | Underlying Disease | Drug Dosage (g)/Duration (days) | Symptoms | Medication Duration Before Symptom Development (days) | Time to Clinical Improvement after Drug Discontinuation (days) | Duration Between Symptom Onset and Initial MRI (days) | Duration Between Drug Discontinuation and Follow-Up MRI (days)[a] |
|---|---|---|---|---|---|---|---|---|
| 1 | 49/M | Crohn disease | 135/90 | Weakness of extremities, dysarthria, gait disturbance | 52 | 10 | 38 | – |
| 2 | 70/M | Brain abscess, LC | 57/38 | Weakness of extremities, dysarthria | 22 | 7 | 7 | 14 |
| 3 | 64/M | Intraabdominal abscess | 37.5/25 | Dysarthria, gait disturbance, visual blurring | 17 | 7 | 17 | 17 |
| 4 | 54/M | Spontaneous bacterial peritonitis, LC | 49.5/33 | Dysarthria, confusion | 15 | 5 | 21 | – |
| 5 | 71/M | DM foot, CRF | 66/44 | Dysarthria, gait disturbance | 37 | 4 | 3 | 34 |
| 6 | 55/M | Ischemic colitis, LC | 21/14 | Dysarthria, gait disturbance, tingling sensation of both extremities | 11 | 7 | 3 | 15 |
| 7 | 61/F | Pseudo-membranous colitis | 40.5/27 | Dysarthria, gait disturbance | 24 | 7 | 5 | – |

**Note:**—LC indicates liver cirrhosis; CRF, chronic renal failure; DM, diabetes mellitus.
[a] Follow-up MR imaging was not studied in 3 patients (patients 1, 4, and 7).

weighted, fast spin-echo T2-weighted, and fast fluid-attenuated inversion-recovery (FLAIR) images were obtained for all patients. Enhanced T1-weighted images with gadopentetate dimeglumine (Magnevist; Schering, Berlin, Germany) administration at 0.1 mmol/kg were also obtained in all patients. Echo-planar DWIs were available for 5 patients. The MR imaging parameters were as follows: 450–66/12/2 (TR/TE/NEX) for spin-echo T1-weighted images, 3666–4000/96–104/1–2/7 (TR/$TE_{eff}$/NEX/echo train) for fast spin-echo T2-weighted images, and 5000–10 000/110–155/2000/1/7 (TR/$TE_{eff}$/TI/NEX/echo train) for fast FLAIR images. The other parameters were the following; section thickness 5–6 mm with a 1.5-mm gap, field of view of 240 mm, and a 256 × 192 matrix. DWI was performed with a single-shot spin-echo echo-planar pulse sequence with 2 diffusion-sensitivity values of 0 and 1000 s/mm$^2$ along all 3 orthogonal axes. From all the DWI sequences, we calculated the apparent diffusion coefficient (ADC) maps.

### *Imaging Analysis*

MR images were retrospectively evaluated by 2 radiologists (D.G.N. and E.K.) by consensus. The anatomic locations of lesions showing hyperintensity on T2-weighted or FLAIR images and lesion enhancements on enhanced T1-weighted images were assessed. Lesion signal intensities were visually assessed on DWI, and ADCs were measured in patients who underwent DWI. Interval changes in brain lesions were assessed in patients with follow-up MR images.

To quantitatively determine the ADC values of lesions, we obtained lesion values by manually drawing regions of interest (ROIs) along lesion boundaries on T2-weighted images. Manually drawn ROIs on T2-weighted images were copied to the same locations on ADC maps. To measure ADC ratios, we also measured ADC values of normal white matter by using ROIs (mean size, 200 mm$^2$) in the subcortical white matter of the frontal lobe.

## Results

### *Demographic and Clinical Data*

Table 1 details the clinical presentation of the 7 patients with MIE. The mean total dose of metronidazole administered was 58.1 g (range, 21–135 g) during a mean period of 38.7 days (range, 14–90 days). The mean duration of medication until the development of neurologic symptoms was 25.4 days (range, 11–52 days). Neurologic symptoms included dysarthria ($n = 7$), gait disturbance ($n = 5$), weakness of the extremities ($n = 2$), mental confusion ($n = 1$), visual disturbance ($n = 1$), and a tingling sensation of the extremities ($n = 1$). Neurologic symptoms improved in all patients within a mean of 6.7 days (range, 4–10 days) after metronidazole discontinuation. Mean duration between symptom onset and initial MR imaging was 13.4 days (range, 3–38 days), and mean duration between medication discontinuation and follow-up MR imaging was 20 days (range, 14–34 days).

### *Lesion Distribution*

Table 2 demonstrates the locations and topographic distributions of lesions seen on T2-weighted and FLAIR images. These images demonstrated bilateral symmetric hyperintense lesions in cerebellar dentate nuclei, midbrain, dorsal pons, medulla, corpus callosum, and cerebral white matter (Figs 1–3). Bilateral symmetric involvements of cerebellar dentate nuclei and midbrain were demonstrated in all patients. Midbrain lesions were in the tectum ($n = 5$, 71%), the tegmentum around periaqueductal gray matter ($n = 4$, 57%), and the red nucleus ($n = 3$, 43%); and lesions of the dorsal pons were in the vestibular nucleus ($n = 6$, 86%), a focal tegmental lesion in the superior olivary nucleus ($n = 6$, 86%), and the abducens nucleus ($n =$

**Table 2: Lesion distribution on T2-weighted and FLAIR MR images in the seven patients with MIE**

| | | Medulla | | Pons | | | Midbrain | | | | |
|---|---|---|---|---|---|---|---|---|---|---|---|
| Patient | Cerebellum (Dentate Nuclei) | Dorsal Medulla | ION | VN | AN | SON | Tectum | Tegmentum | RN | Corpus Callosum | Subcortical WM |
| 1 | + | − | − | + | + | + | − | + | + | − | − |
| 2 | + | − | − | + | − | + | + | + | + | + | − |
| 3 | + | + | + | + | − | + | + | + | − | + | + |
| 4 | + | + | − | + | + | + | − | + | + | + | − |
| 5 | + | + | − | + | + | + | + | − | − | − | − |
| 6 | + | + | − | + | + | + | + | − | − | + | − |
| 7 | + | − | − | − | − | − | + | − | − | − | − |

**Note:**—WM indicates white matter; ION, inferior olivary nucleus; VN, vestibular nucleus; AN, abducens nucleus; SON, superior olivary nucleus; RN, red nucleus; +, presence of lesion at each anatomic location; −, no abnormality on MR at each anatomic location.

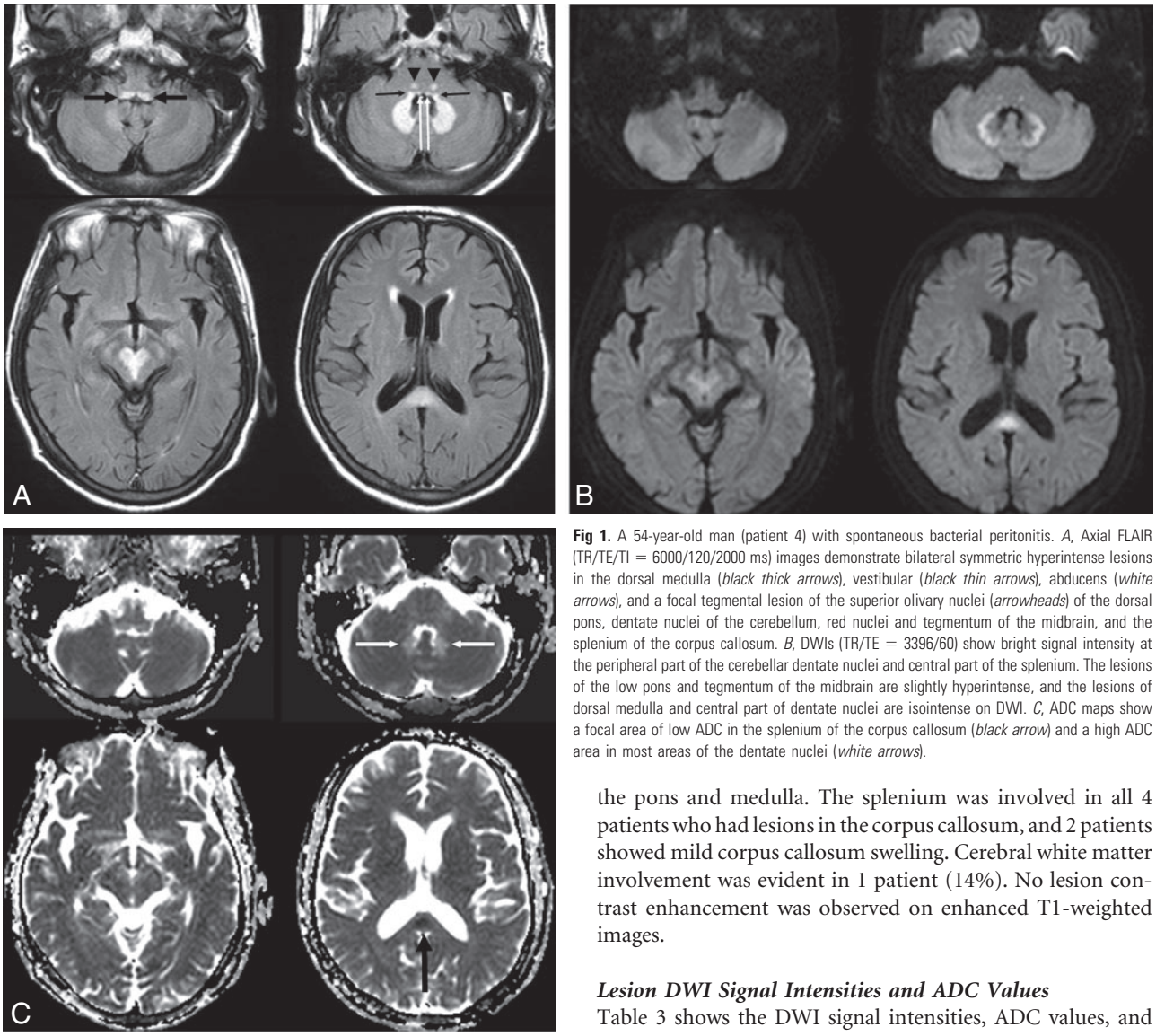


**Fig 1.** A 54-year-old man (patient 4) with spontaneous bacterial peritonitis. *A*, Axial FLAIR (TR/TE/TI = 6000/120/2000 ms) images demonstrate bilateral symmetric hyperintense lesions in the dorsal medulla (*black thick arrows*), vestibular (*black thin arrows*), abducens (*white arrows*), and a focal tegmental lesion of the superior olivary nuclei (*arrowheads*) of the dorsal pons, dentate nuclei of the cerebellum, red nuclei and tegmentum of the midbrain, and the splenium of the corpus callosum. *B*, DWIs (TR/TE = 3396/60) show bright signal intensity at the peripheral part of the cerebellar dentate nuclei and central part of the splenium. The lesions of the low pons and tegmentum of the midbrain are slightly hyperintense, and the lesions of dorsal medulla and central part of dentate nuclei are isointense on DWI. *C*, ADC maps show a focal area of low ADC in the splenium of the corpus callosum (*black arrow*) and a high ADC area in most areas of the dentate nuclei (*white arrows*).

4, 57%).[18] Lesions of the medulla were in the vestibular nucleus of the dorsal medulla ($n$ = 4, 57%) and the inferior olivary nucleus ($n$ = 1, 14%). In 6 (86%) patients, MR images showed a characteristic pattern of bilateral symmetric involvement of the dentate nuclei, vestibular nuclei, and a focal area of the tegmentum in the superior olivary nucleus at the level of the low pons (Figs 1 and 2). Dorsal parts of the pons and medulla were always involved in all patients who had lesions in the pons and medulla. The splenium was involved in all 4 patients who had lesions in the corpus callosum, and 2 patients showed mild corpus callosum swelling. Cerebral white matter involvement was evident in 1 patient (14%). No lesion contrast enhancement was observed on enhanced T1-weighted images.

### *Lesion DWI Signal Intensities and ADC Values*

Table 3 shows the DWI signal intensities, ADC values, and ADC ratios of lesions on initial MR imaging in 5 patients (patients 1 and 4–7) and follow-up MR imaging in 1 patient (patient 6). DWI signal intensities were variable, from hyperintense to isointense in lesions of the dentate nucleus, midbrain, medulla, and pons (Figs 1 and 2). The lesions of the corpus callosum were hyperintense (Figs 1 and 2). Mean ADC and ADC ratio values of the splenium were $515 \times 10^{-6}$ mm$^2$/s and 0.7, respectively. Although the ADC values of lesions of the dentate nucleus, midbrain, medulla, and pons were similar or

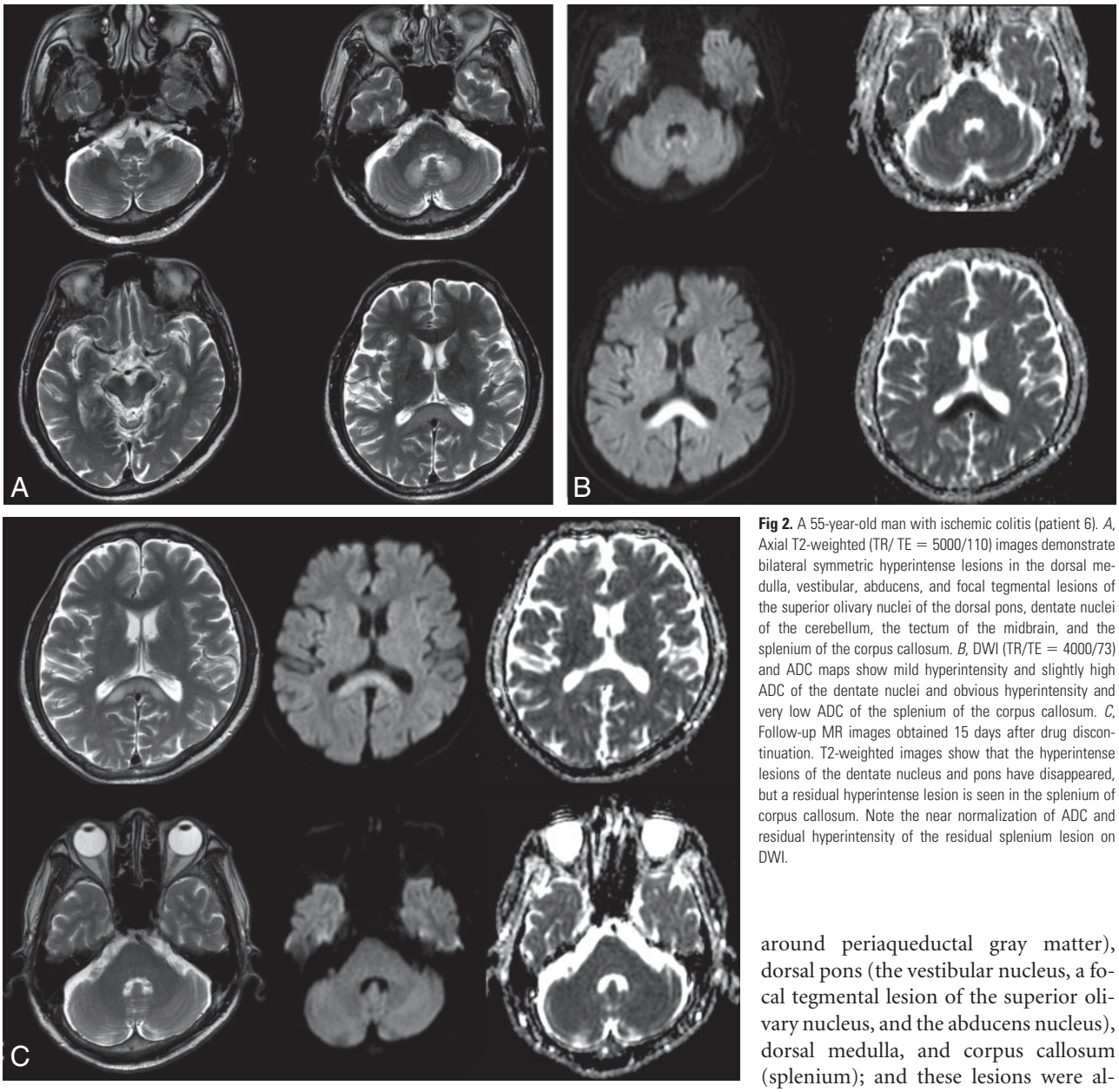


**Fig 2.** A 55-year-old man with ischemic colitis (patient 6). *A*, Axial T2-weighted (TR/ TE = 5000/110) images demonstrate bilateral symmetric hyperintense lesions in the dorsal medulla, vestibular, abducens, and focal tegmental lesions of the superior olivary nuclei of the dorsal pons, dentate nuclei of the cerebellum, the tectum of the midbrain, and the splenium of the corpus callosum. *B*, DWI (TR/TE = 4000/73) and ADC maps show mild hyperintensity and slightly high ADC of the dentate nuclei and obvious hyperintensity and very low ADC of the splenium of the corpus callosum. *C*, Follow-up MR images obtained 15 days after drug discontinuation. T2-weighted images show that the hyperintense lesions of the dentate nucleus and pons have disappeared, but a residual hyperintense lesion is seen in the splenium of corpus callosum. Note the near normalization of ADC and residual hyperintensity of the residual splenium lesion on DWI.

higher than those of normal white matter, ADC values were lower in corpus callosum lesions than in normal white matter.

### *Reversibility of Lesions*

Hyperintense lesions on T2-weighted and FLAIR images were found to be completely reversible in follow-up MR images in 3 patients (Fig 3) and partially reversible in 1 patient (Fig 2). In 1 of 3 patients with lesions of the corpus callosum, focal residual hyperintensities were observed only in the splenium on follow-up MR images (Fig 2). Lesions other than in the corpus callosum had disappeared in all 4 patients at follow-up MR imaging. No lesion was found not to have changed or increased by follow-up MR imaging.

## Discussion

Our study demonstrates that the typical locations of lesions by MR imaging in patients with MIE are the cerebellar dentate nuclei, midbrain (tectum, red nucleus, and tegmentum around periaqueductal gray matter), dorsal pons (the vestibular nucleus, a focal tegmental lesion of the superior olivary nucleus, and the abducens nucleus), dorsal medulla, and corpus callosum (splenium); and these lesions were always bilateral and symmetric. Uncommon locations were the inferior olivary nucleus and the white matter of the cerebral hemispheres.

Lesions of the cerebellar nuclei, olivary nuclei, and brain stem as demonstrated on MR images in patients with MIE are explained by the histologic findings of previous experimental animal studies.[19-22] A toxicologic study[19] in rats demonstrated well-demarcated usually symmetric lesions in the vestibular nuclei, cochlear nuclei, rostral colliculus, cerebellar nuclei, and olivary nuclei after the administration of high doses of metronidazole, and these lesions were characterized as spongiform changes within neurons. A similar experimental study in dogs demonstrated the degeneration and selective loss of Purkinje cells[20] and mild swelling of axon sheaths in vestibular-cerebellar white matter tracts and leukomalacia near the vestibular nerve radix.[21] According to a recent study in cats, multifocal well-demarcated foci of necrosis were present in central brain stem regions from the diencephalon to the medulla oblongata.[22] However, no documented data are available

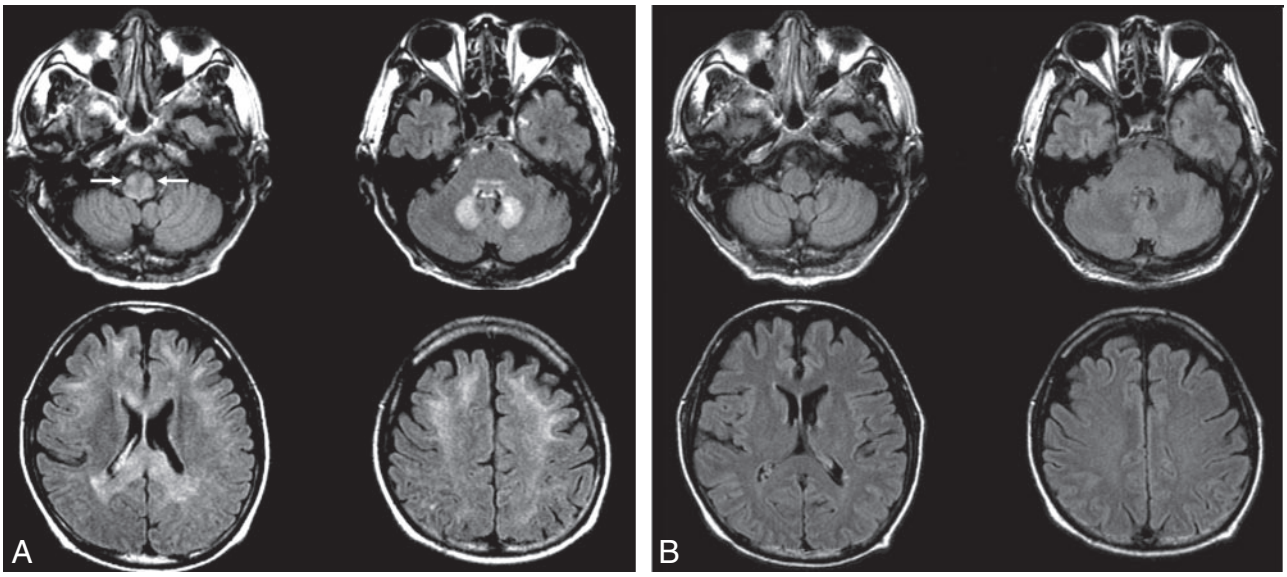


**Fig 3.** A 64-year-old man with an intra-abdominal abscess (patient 3). *A*, Axial FLAIR (TR/TE/TI = 10,000/122/2000) images show bilateral symmetric hyperintense lesions in the inferior olivary nuclei (*arrows*) and dorsal medulla, dorsal pons, cerebellar dentate nuclei, splenium and genu of corpus callosum, and subcortical white matter of both cerebral hemispheres. *B*, Follow-up FLAIR images obtained 17 days after drug discontinuation show complete reversal of all lesions.

**Table 3: Signal intensities and ADC values of lesions of DWI on initial MR imaging in five patients and follow-up MR imaging in one patient**

| Lesions | Signal Intensity on DWI (High/ Mixed/Iso) | ADC Value ($10^{-6}$ mm$^2$/s) | ADC Ratio[a] |
|---|---|---|---|
| Initial patients ($n$ = 5) | | | |
| Cerebellar dentate nucleus ($n$ = 5) | 2/2/1 | 885 ± 67 | 1.2 ± 0.06 |
| Midbrain ($n$ = 5) | | | |
| Tectum ($n$ = 3) | 2/0/1 | 872 ± 59 | 1.1 ± 0.10 |
| Red nucleus ($n$ = 2) | 1/1/0 | 929 ± 2 | 1.3 ± 0.01 |
| Tegmentum around periaqueductal GM ($n$ = 2) | 2/0/0 | 1021 ± 59 | 1.5 ± 0.09 |
| Dorsal pons ($n$ = 4) | 2/0/2 | 844 ± 75 | 1.1 ± 0.16 |
| Dorsal medulla ($n$ = 3) | 1/1/1 | 959 ± 162 | 1.3 ± 0.25 |
| Splenium ($n$ = 2) | 2/0/0 | 515 ± 195 | 0.7 ± 0.30 |
| Follow-up patient ($n$ = 1) | | | |
| Cerebellar dentate nucleus ($n$ = 1) | (0/0/1) | 734 | 1.0 |
| Splenium ($n$ = 1) | (1/0/0) | 1097 | 1.4 |

**Note:**—Iso indicates isointense; GM, gray matter.
[a] ADC values and ratios are presented as mean ± SD. ADC ratio is the ratio of the ADC value of a lesion to that of normal subcortical white matter.

on histologic changes in hemispheric white matter, corpus callosum, and basal ganglia in experimentally induced metronidazole neurotoxicity.

According to the previously reported 13 cases of MIE,[7-16] cerebellar dentate nuclei are most commonly involved on MR images, and this was found in 100% of our 7 cases and in 10 of the 13 previously reported cases. Less common locations included the corpus callosum ($n$ = 6), midbrain ($n$ = 4), basal ganglia ($n$ = 4), and cerebral subcortical white matter ($n$ = 4). Previous reports have also found involvements of the dorsal medulla ($n$ = 2), dorsal pons ($n$ = 1), inferior olivary nuclei ($n$ = 1), and anterior commissure ($n$ = 1). The accumulated data of our cases and previously reported cases show that the lesion distribution of MIE is as follows: cerebellar dentate nuclei ($n$ = 17, 85%), midbrain ($n$ = 11, 55%), corpus callosum ($n$ = 10, 50%), pons ($n$ = 7, 35%), medulla ($n$ = 6, 30%), and subcortical white matter of the hemisphere ($n$ = 5, 25%) and basal ganglia ($n$ = 4, 20%) in a total of 20 patients of our cases and previously reported cases.

Although the anatomic detail of brain stem lesions was not described by previous case reports, the present study demonstrates topographic distributions of lesions in the midbrain, pons, and medulla on MR imaging. Midbrain lesions involved the tectum, tegmentum, and red nucleus; and structural involvements varied. For the lesion in the pons, MR images showed a characteristic pattern of vestibular and abducens nuclei of the dorsal pons and a focal tegmental lesion of the superior olivary nucleus at the level of the low pons. All 4 patients with medullary lesions showed a linear T2 hyperintense lesion of the vestibular nuclei of the floor of the fourth ventricle at the dorsal medulla. The findings of the present study and of previous studies suggest that patients with MIE share characteristic MR imaging lesion features and distributions. First, lesions are always symmetric and bilateral, which is a typical pattern of metabolic encephalopathy. Second, bilateral cerebellar dentate nuclei are involved in most cases. Third, the MR imaging feature of bilateral symmetric lesions in the dentate nuclei, vestibular nuclei, and a focal tegmental lesion in the superior olivary nuclei of the low pons is a characteristic pattern in patients with lesions of the pons. Fourth, lesions of the corpus callosum always involve the splenium.

The involvement of the inferior olivary nucleus in MIE has previously been reported in only 1 patient.[12] Seok et al[12] observed that increased signal intensity of the inferior olivary nuclei did not change during follow-up MR imaging, whereas that of other lesions disappeared. They suggested that a lesion of the inferior olivary nucleus may be inferred to be the result of lesions that interrupt the circuit of the Guillain-Mollaret triangle, rather than being a result of lesions induced by met-

ronidazole therapy. However, in 1 patient (Fig 3) of the present study, the lesions of the bilateral olivary nuclei and other lesions disappeared at follow-up MR imaging performed after drug discontinuation. It is unclear whether lesions of the inferior olivary nuclei in MIE are caused by direct neurotoxic injury by metronidazole or by hypertrophic olivary degeneration.

Diffusion changes of lesions in patients with MIE are somewhat controversial. The previous case reports[11,12,14] suggested vasogenic edema of the lesions in the cerebellar dentate nuclei and cytotoxic edema of lesions in the internal capsule, anterior commissure, splenium, and subcortical white matter. In the present study, DWI showed increased ADC value and vasogenic edema in lesions of the midbrain, pons, medulla, and cerebellar dentate nuclei, which involve mainly gray matter, but decreased ADC value and cytotoxic edema in lesions of the corpus callosum. Some lesions showing DWI hyperintensity and no low ADC value could be explained by T2 shinethrough effect.

Although it is unclear why lesion ADC values depend on lesion location, we presume that mechanisms of metronidazole neurotoxicity may differ for white matter lesions and lesions predominantly of gray matter. However, because heterogeneous DWI signal intensities in lesions showing T2 hyperintensity were observed in some patients, it could be that lesion ADC values might simply reflect differences in degrees of edema, whether vasogenic or cytotoxic in nature. Moreover, diffusion signal-intensity change may be also related to the stage of neurotoxic injury and the time interval lapsed between initial and follow-up MR imaging. The present study shows incomplete resolution of a lesion of the splenium of the corpus callosum in only 1 patient, in whom this lesion had a very low ADC value ($377 \times 10^{-6}$ mm$^2$/s) (Fig 2). In the other patient who had a splenial lesion on the initial DWI, the ADC value of the lesion was also low ($653 \times 10^{-6}$ mm$^2$/s); however, the reversibility of the lesion could not be assessed due to no follow-up DWI.

Previous studies[4-6] have suggested several mechanisms of metronidazole neurotoxicity, ie, the RNA binding,[4] DNA binding[5] of intermediate metabolites of metronidazole, and the modulation of the inhibitory neurotransmitter g-aminobutyric acid receptor within the cerebellar and vestibular systems.[6] Although the mechanism of metronidazole neurotoxicity remains unclear, most lesions induced by metronidazole neurotoxicity may be wholly reversible.

Acute Wernicke encephalopathy is the most important disease in the differential diagnosis of MIE. Acute Wernicke encephalopathy and MIE may be clinically confused during the early clinical stage because MIE may produce similar clinical conditions and symptoms. The MR imaging features of MIE may also mimic Wernicke encephalopathy. Typically the MR imaging features of acute Wernicke encephalopathy are bilateral symmetric T2 hyperintense lesions in the periventricular regions of the mammillary body, medial thalamus, floors of the third and fourth ventricles, periaqueductal gray matter, and midbrain tectum.[23] Less common MR imaging features of Wernicke encephalopathy include the involvements of pericentral cortices,[24] basal ganglia,[24] and the superior cerebellar vermis.[25,26] Recently, Bae et al[27] and Kang et al[28] reported 2 cases of acute nonalcoholic Wernicke encephalopathy with atypical MR imaging features. These 2 cases had almost the same MR imaging feature of bilateral symmetric lesions at the dentate nuclei, vestibular nuclei, and at focal areas of the tegmentum. This MR imaging feature was not reported by previous studies of Wernicke encephalopathy, and it is consistent with MR imaging findings of MIE, as documented by the present study. In the previously mentioned case reports,[27,28] metronidazole had been administrated for a prolonged period until symptoms developed (S.J. Bae and G. Choi, personal communications, December 2006), and the authors did not rule out the possibility of MIE. Therefore, it is unclear whether the previously reported atypical MR imaging features were due to acute Wernicke encephalopathy or MIE or both. Although lesions of the cerebellar vermis reported in Wernicke encephalopathy[25,26] are explained by histologic cerebellar changes found in this condition, lesions of cerebellar dentate nuclei are not supported by pathology studies on Wernicke encephalopathy.[29,30]

Although MR imaging findings of bilateral involvement of the dentate nuclei are a very characteristic feature of MIE, the differential diagnosis of T2 hyperintense lesions of the bilateral cerebellar dentate nuclei in patients with symptoms of acute encephalopathy includes methyl bromide intoxication,[31] maple syrup urine disease,[32] and enteroviral encephalomyelitis.[33] Brain stem lesions of metronidazole neurotoxicity should be differentiated from those of central pontine myelinolysis with or without extrapontine myelinolysis. Whereas pontine myelinolysis involves the basis pontis and may show restricted diffusion of pons lesions on DWI,[34] MIE affects the dorsal pons region and has no restricted diffusion on DWI in most cases. The differential diagnosis of T2 hyperintense focal lesions in the corpus callosum splenium includes various demyelinating diseases (eg, Marchiafava-Bignami disease, encephalitis, osmotic myelinolysis, and transient splenial lesions). The etiologies of transient T2 hyperintense focal lesions in the splenium of the corpus callosum include patients with epilepsy treated with antiepileptic drugs,[35] acute infectious encephalitis (influenza, *Escherichia coli*, mumps, adenovirus, Epstein-Barr virus, and Rota virus),[36-39] demyelinating lesions including osmotic myelinolysis, and acute toxic encephalopathy (methotrexate and 5-fluorouracil).[40-41]

The present study has several limitations. First, the number of patients included was small, and follow-up MR images were obtained in a limited number of patients. Second, further study is needed to determine the clinical significance of lesion ADC values with respect to the prediction of clinical outcome.

## Conclusion

The brain lesions demonstrated on MR images in MIE were always bilateral and symmetric and were typically located at the cerebellar dentate nuclei, dorsal medulla, dorsal pons, midbrain, and splenium of the corpus callosum. Uncommon lesion locations were the inferior olivary nucleus of the medulla and white matter of the cerebral hemispheres. According to DWI, most of the lesions in MIE probably correspond to areas of vasogenic edema, whereas only some of them, located in the corpus callosum, correspond to cytotoxic edema.

## References


1. Freeman CD, Klutman NE, Lamp KC. **Metronidazole: a therapeutic review and update.** *Drugs* 1997;54:679–708
2. Frytak S, Moertel CH, Childs DS. **Neurologic toxicity associated with high-dose metronidazole therapy.** *Ann Intern Med* 1978;88:361–62
3. Snavely SR, Hodges GR. **The neurotoxicity of antibacterial agents.** *Ann Intern Med* 1984;101:92–104
4. Bradley WG, Karlsson IJ, Rassol CG. **Metronidazole neuropathy.** *BMJ* 1977;2:610–11
5. Wright KH, Tyler JW. **Recognizing metronidazole toxicosis in dogs.** *Vet Med* 2003;98:410–18
6. Evans J, Levesque D, Knowles K, et al. **Diazepam as a treatment for metronidazole toxicosis in dogs: a retrospective study of 21 cases.** *J Vet Intern Med* 2003;17:304–10
7. Ahmed A, Loes DJ, Bressler EL. **Reversible resonance imaging findings in metronidazole-induced encephalopathy.** *Neurology* 1995;45:588–89
8. Cecil KM, Halsted MJ, Schapiro M, et al. **Reversible MR imaging and MR spectroscopy abnormalities in association with metronidazole therapy.** *J Comput Assist Tomogr* 2002;26:948–51
9. Horlen CK, Seifert CF, Malouf CS. **Toxic metronidazole-induced MRI changes.** *Ann Pharmacother* 2000;34:1273–75
10. Woodruff BK, Wijdicks EF, Marshall WF. **Reversible metronidazole-induced lesions of the cerebellar dentate nuclei.** *N Engl J Med* 2002;346:68–69
11. Heaney CJ, Campeau NG, Lindell EP. **MR imaging and diffusion-weighted imaging changes in metronidazole (Flagyl)-induced cerebellar toxicity.** *AJNR Am J Neuroradiol* 2003;24:1615–17
12. Seok JI, Yi H, Song YM, et al. **Metronidazole-induced encephalopathy and inferior olivary hypertrophy.** *Arch Neurol* 2003;60:1796–800
13. Ito H, Maruyama M, Ogura N, et al. **Reversible cerebellar lesions induced by metronidazole therapy for helicobacter pylori.** *J Neuroimaging* 2004;14:369–71
14. Kim DW, Park JM, Yoon BW, et al. **Metronidazole-induced encephalopathy.** *J Neurol Sci* 2004;224:107–11
15. Kim KH, Choi JW, Lee JY, et al. **Two cases of metronidazole-induced encephalopathy.** *Korean J Gastroenterol* 2005;45:195–200
16. De Bleecker JL, Leroy BP, Meire VI. **Reversible visual deficit and corpus callosum lesions due to metronidazole toxicity.** *Eur Neurol* 2005;53:93–95
17. Karch FE, Lasagna L. **Adverse drug reactions: a critical review.** *JAMA* 1975;234:1236–41
18. Duvernoy HM. *Human Brain Stem Vessels.* 2nd ed. Berlin, Germany: Springer-Verlag; 1999:60–81
19. von Rogulja P, Kovac W, Schmid H. **Metronidazole encephalopathy in rats.** *Acta Neuropathol (Berl)* 1973;25:36–45
20. Scharer K. **Selective injury to Purkinje cells in the dog after oral administration of high-dose of nitroimidazole derivates** [in German]. *Verh Dtsch Ges Pathol* 1972;56:407–10
21. Dow SW, LeCouteur RA, Poss ML, et al. **Central nervous system toxicosis associated with metronidazole treatment of dogs: five cases (1984–1987).** *J Am Vet Med Assoc* 1989;195:365–68
22. Olson EJ, Morales SC, McVey AS, et al. **Putative metronidazole neurotoxicosis in a cat.** *Vet Pathol* 2005;42:665–69
23. Gallucci M, Bozzao A, Splendiani A, et al. **Wernicke encephalopathy: MR findings in five patients.** *AJR Am J Roentgenol* 1990;155:1309–14
24. Doss A, Mahad D, Romanowski CAJ. **Wernicke encephalopathy: unusual findings in nonalcoholic patients.** *J Comput Assist Tomogr* 2003;27:235–40
25. Murata T, Fujito T, Kimura H, et al. **Serial MRI and (1)H-MRS of Wernicke's encephalopathy: report of a case with remarkable cerebellar lesions on MRI.** *Psychiatry Res* 2001;108:49–55
26. Lapergue B, Klein I, Olivot JM, et al. **Diffusion-weighted imaging of cerebellar lesions in Wernicke's encephalopathy.** *J Neuroradiol* 2006;33:126–28
27. Bae SJ, Lee HK, Lee JH, et al. **Wernicke's encephalopathy: atypical manifestation at MR imaging.** *AJNR Am J Neuroradiol* 2001;22:1480–82
28. Kang SY, Kang JH, Choi JC, et al. **Wernicke's encephalopathy: unusual manifestation on MRI.** *J Neurol* 2005;252:1550–52
29. Troncoso JC, Johnston MV, Hess KM, et al. **Model of Wernicke's encephalopathy.** *Arch Neurol* 1981;38:350–54
30. Mulholland PJ. **Susceptibility of the cerebellum to thiamine deficiency.** *Cerebellum* 2006;5:55–63
31. Geyer HL, Schaumburg HH, Herskovitz S. **Methyl bromide intoxication causes reversible symmetric brainstem and cerebellar MRI lesions.** *Neurology* 2005;64:1279–81
32. Jan W, Zimmerman RA, Wang ZJ, et al. **MR diffusion imaging and MR spectroscopy of maple syrup urine disease during acute metabolic decompensation.** *Neuroradiology* 2003;45:393–99
33. Shen WC, Chiu HH, Chow KC, et al. **MR imaging findings of enteroviral encephalomyelitis: an outbreak in Taiwan.** *AJNR Am J Neuroradiol* 1999;20:1889–95
34. Cramer SC, Stegbauer KC, Schneider A, et al. **Decreased diffusion in central pontine myelinolysis.** *AJNR Am J Neuroradiol* 2001;22:1476–79
35. Uchino A, Takase Y, Nomiyama K, et al. **Acquired lesions of the corpus callosum: MR imaging.** *Eur Radiol* 2006;16:905–14
36. Bulakbasi N, Kocaoglu M, Tayfun C, et al. **Transient splenial lesion of the corpus callosum in clinically mild influenza-associated encephalitis/encephalopathy.** *AJNR Am J Neuroradiol* 2006;27:1983–86
37. Hagemann G, Mentzel HJ, Weisser H, et al. **Multiple reversible MR signal changes caused by Epstein-Barr virus encephalitis.** *AJNR Am J Neuroradiol* 2006;27:1447–49
38. Kobata R, Tsukahara H, Nakai A, et al. **Transient MR signal changes in the splenium of the corpus callosum in rotavirus encephalopathy: value of diffusion-weighted imaging.** *J Comput Assist Tomogr* 2002;26:825–28
39. Maeda M, Tsukahara H, Terada H, et al. **Reversible splenial lesion with restricted diffusion in a wide spectrum of diseases and conditions.** *J Neuroradiol* 2006;33:229–36
40. Sandoval C, Kutscher M, Jayabose S, et al. **Neurotoxicity of intrathecal methotrexate: MR imaging findings.** *AJNR Am J Neuroradiol* 2003;24:1887–90
41. Lucato LT, McKinney AM, Short J, et al. **Reversible findings of restricted diffusion in 5-fluorouracil neurotoxicity.** *Australas Radiol* 2006:50:364–68